

Soil-foundation interaction model for the assessment of tunnelling-induced damage to masonry buildings

Burd, H.J.¹, Yiu, W.N.¹, Acikgoz, S.¹ & Martin, C.M.¹

¹Department of Engineering Science, University of Oxford, Oxford, UK.

Corresponding author – H.J. Burd. email *harvey.burd@eng.ox.ac.uk*

Abstract

Shallow tunnel construction inevitably causes local ground movements to occur. In an urban environment, these ground movements may cause damage to existing buildings on the ground surface. This paper describes a new, simplified, one-dimensional (1D) soil-foundation interaction model for use in damage assessment analyses of buildings that are at risk of tunnelling-induced damage. Simplified models of this sort facilitate efficient building risk assessments for urban infrastructure projects. The proposed soil-foundation interaction model is intended principally for buildings with traditional load-bearing masonry construction founded on embedded shallow foundations. A nonlinear Winkler model (incorporating shear and normal tractions acting on the foundation and the possibility of frictional sliding and gapping beneath the footing) is used to represent the soil-foundation interaction; the model also provides a means of specifying the tunnel-induced ground movements. The soil-foundation interaction model is demonstrated by combining it with a 2D plane stress model of a building facade; the combined model is shown to provide a close representation of the response of the facade to tunnel-induced ground movements, as computed with a corresponding 3D finite element model, but at a small fraction of the computational cost.

Keywords: Masonry; Building damage; Tunnelling; Soil-structure interaction; Foundations; Nonlinear Winkler model

1.0 Introduction

Tunnel construction processes inevitably cause local ground movements to occur. During the planning and design of tunnel construction activities in urban areas (e.g. for new infrastructure projects) consideration needs to be given to the response of any existing buildings that may be affected by construction-induced ground movements, to assess the risk of structural damage. Buildings of traditional masonry construction are especially vulnerable to forms of settlement damage that range from minor, unsightly, cracking through to significant building distortions.

Routine risk assessments for tunnel-induced settlement damage to buildings follow established procedures (e.g. Mair et al. 1996; Burland 2001). These procedures rely on estimates of the greenfield tunnel-induced displacements (i.e. the ground movements that are considered likely to occur in the absence of existing infrastructure). For single tunnels these estimates typically employ Gaussian functions (Peck 1969; Mair & Taylor 1997). For multiple tunnels, a commonly-employed approach is to combine the estimated greenfield displacements for each tunnel by superposition (e.g. Rankin 1988; Divall et al. 2012; Ocaik 2014). Alternatively, greenfield displacements can be predicted using finite element methods (e.g. Addenbrooke and Potts 2001).

For masonry buildings supported on shallow foundations, routine damage risk assessments typically begin with a simplified modelling approach in which the building facades are represented as isolated elastic flexible beams (Burland & Wroth 1974; Boscardin & Cording 1989) deforming according to the estimated foundation-level greenfield displacements. Damage classification metrics based on the maximum tensile strain induced in the building as estimated from the model (e.g. Burland 2001; Mair et al. 1996) are typically employed. Although this provides a rapid ‘screening’ process, it is unlikely to deliver realistic estimates of the actual behaviour of the building, since the building stiffness will typically cause the local tunnel-induced displacements to depart significantly from the greenfield values. Additionally, features such as openings for windows and doors (Yiu et al. 2017a), pre-existing damage (Acikgoz et al. 2021) and nonlinear behaviour of the masonry (Giardina et al. 2013) are likely to cause the induced tensile strains in the building to depart significantly from those implied by the elastic flexible beam assumption.

In special cases (e.g. high heritage-value and/or especially vulnerable buildings) it may be appropriate to employ detailed, fully-coupled 3D finite element models – incorporating the tunnelling processes, the soil and the building – in risk assessment calculations. However, routine assessments for urban infrastructure projects typically rely on simplified procedures to assess large numbers of buildings, efficiently, within project timescales. In cases where the basic isolated elastic flexible beam approach is considered insufficient, assessments are therefore typically based on ‘semi-coupled’ models, where the soil-structure interaction is represented by simplified structural and/or geotechnical models. Models employing simplified equivalent beam and equivalent solid structural models (Pickhaver et al. 2010; Losacco et al. 2014) facilitate explicit analysis of tunnelling-induced ground movements and soil-foundation interactions. However, to predict strain in buildings (relevant to standard approaches in which tensile strain magnitude is correlated to severity of

damage), the computed displacement fields subsequently need to be applied to separate, more detailed, structural models.

Alternative semi-coupled approaches have been developed employing simplified geotechnical (rather than structural) models while adopting high-fidelity models for the structure. In the modelling approach described in Giardina et al. (2013), for example, the combined mechanics of the soil and the soil-foundation interaction are represented by one-dimensional (1D) interface elements incorporating specified elastic/frictional characteristics. This interface element modelling approach provides a convenient means of incorporating the greenfield displacements in the analysis; this is achieved by prescribing the greenfield displacements to the bottom set of interface element nodes. The interface elements then interact with the structure to facilitate the direct calculation of the building displacements and strains, incorporating the influence of soil-structure interaction mechanisms.

Semi-coupled approaches incorporating simplified geotechnical models conveniently reduce the size of the problem. However, the accuracy of this type of model depends on the level of sophistication employed in the idealisations of the soil and foundation components, and their interactions. Specifically, it is desirable that these components should be able to account for nonlinear soil behaviour and potential gapping and sliding mechanisms in the soil-foundation interaction. 3D finite element studies by Yiu et al. (2017b) highlighted that the width and embedment depth of the strip footing, and the frictional characteristics of the soil-footing interface, can have a significant influence on the severity of the predicted damage; effective soil-foundation interaction models need to be able to address these critical aspects. Past studies (e.g. Deck & Singh 2012; Camós et al. 2014; Dalgic et al. 2018; Basmaji et al. 2019) employed simple Winkler or Pasternak geotechnical models; such models omit potentially significant non-local interactions between the foundation and the ground. More sophisticated formulations which consider non-local interactions in the soil, employing elastic half-space solutions and gapping and sliding mechanisms incorporating elasto-plastic models, were proposed for surface structures by Franza and DeJong (2019) and Elkayam and Klar (2019). However, these models do not consider the important influence of foundation embedment, and nonlinear soil behaviour is necessarily treated in an approximate manner. Moreover, suitable half-space solutions may not be available for the layered - or otherwise nonhomogeneous - soils that are commonly encountered in practical cases.

The current paper describes a new general-use 1D soil-foundation (geotechnical) model and associated calibration methods. The model is based on a Winkler approach; although this modelling procedure does not incorporate spatial coupling within the soil it is able to incorporate other significant aspects of the problem. The model is intended to be combined with detailed structural models to facilitate reliable and efficient semi-coupled analyses for damage risk assessment purposes. The model has two components: (i) a strip footing model, and (ii) a soil-foundation interaction model. The strip footing is a linear elastic component with a specified axial stiffness but zero stiffness in bending. The separate soil-foundation interaction model represents nonlinear soil- footing interaction behaviour, including the potential for gapping beneath the footing and frictional sliding; the model also provides a direct means of specifying the tunnel-induced ground movements via prescribed greenfield displacements. The decision to neglect bending effects in the strip footing model rests on a range of prior numerical experiments that demonstrate that the influence of the bending action of the footing is typically very small compared with its tie action. (Neglecting bending effects in the footing has the additional benefit - from an implementation perspective - that a beam formulation, which would require the introduction of additional rotational degrees of freedom, is not required).

The 1D soil-foundation model is demonstrated by combining it with a simplified building model comprising two-dimensional (2D) elastic plane stress finite elements. The resulting combined model is referred to as 'S2M' (Simplified 2D assessment Model). The S2M is implemented in bespoke code written in MATLAB. Damage assessment metrics are determined from the S2M via a 'characteristic tunnel-induced tensile strain', ε_{99}^t , defined as the tensile strain that is exceeded in only 1% of the area of the facade or wall being modelled (Yiu et al. 2017a). The adoption of the characteristic strain as an indicator of structural damage resolves the issue of mesh dependency in the computed strains near to the corners of any openings in the facade. The characteristic strain is considered to map directly onto the damage correlations that are employed in routine assessments (e.g. Burland 2001).

The paper is organised as follows. In Section 2, the formulation of the S2M is described. Techniques to calibrate the model are discussed in Section 3. Section 4 develops S2M models to investigate tunnel-induced damage for building geometries explored in earlier work (Yiu et al. 2017a; Giardina et al. 2013). The predictive performance of the S2M is evaluated by comparisons with fully-coupled '3D finite element reference analyses' in which the same structural model is employed but the soil and the construction of the tunnel are modelled explicitly. To further assess the S2M, Section 5

explores how specific aspects of the 1D soil-foundation interaction model influence the predicted damage severity. Section 6 presents a discussion on the use of the S2M in engineering practice, highlighting its advantages over similar approaches, and providing an evaluation of its limitations. Conclusions are provided in Section 7.

2.0 Formulation of the simplified 2D assessment model (S2M)

2.1 Problem specification

The proposed formulation is based on the problem specified in Fig. 1. This incorporates an ‘isolated facade’ idealisation of a masonry building facade or wall founded on a strip footing of width b_{foot} embedded in the soil to a depth $d_{\text{base}} = d_{\text{top}} + d_{\text{foot}}$. In the following discussion, the 2D building model is referred to as a masonry ‘panel’. The adopted ground conditions – intended to be representative of geotechnical conditions in London – comprise a surface layer of Terrace gravel above the deeper-lying London clay. The phreatic surface is assumed to lie well below the base of the footing. This geotechnical and foundation configuration has been chosen to be consistent with the prior 3D finite element studies on tunnel-soil-building interaction by Yiu et al. (2017a); this facilitates the adoption of the modelling procedures in Yiu et al. (2017a) as the basis of the 3D finite element reference analyses used to gauge the veracity of the proposed 1D soil-foundation model. However, the proposed soil-foundation model is applicable to other geotechnical conditions and strip footing geometries.

An arbitrary arrangement of shallow tunnels (considered to be orthogonal to the plane of the masonry panel in the current model, see Fig. 1a) is constructed near to the panel. Fig. 1 also illustrates the strip footing and the soil-foundation interaction model – implemented in the S2M as 1D finite elements – positioned at the mid-depth of the strip footing. In the current S2M implementation, the panel is represented with conventional 2D elastic plane stress finite elements, but the 1D soil-foundation model is also suitable for coupling with other forms of structural model.

The footing material is specified to have the same unit weight, γ_s , as the Terrace gravel in which it is embedded. This facilitates the specification of a simple geostatic stress system in which the S2M (and, as described in Section 4, the 3D reference analyses) are initiated with the panel absent from the model, but with the footing pre-embedded in the soil. In this initial geostatic state, the line tractions (force per unit length) considered to be applied to the footing surfaces (Fig. 1c) in the S2M are $p_{\text{top}} = \gamma_s d_{\text{top}} b_{\text{foot}}$, $p_{\text{side}} = K_0 \gamma_s (d_{\text{top}} + d_{\text{foot}}/2) d_{\text{foot}}$, $p_{\text{base}} = \gamma_s d_{\text{base}} b_{\text{foot}}$ where K_0 is the coefficient of lateral earth pressure. Consistent with the 3D reference analyses, the value of K_0

adopted in the S2M is $K_0 = 1 - \sin(35^\circ) = 0.426$. The net vertical line traction, t_v , applied by the soil to the foundation (positive downwards, Fig. 1d) is $t_v = p_{\text{top}} + w_{\text{foot}} - p_{\text{base}}$ where w_{foot} is the weight of the footing per unit length ($w_{\text{foot}} = \gamma_s d_{\text{foot}} b_{\text{foot}}$). In the initial geostatic state $t_v = 0$. A net horizontal traction, t_h , comprising the summation of the lateral tractions on all four sides of the footing (Fig. 1c), is assumed to act on the foundation.

2.2 Virtual work statement for the S2M

A virtual work statement for the S2M, with reference to the geostatic stress state, is,

$$\delta W_E = \delta W_I \quad (1)$$

The external virtual work δW_E (associated with gravity loading on the panel) is,

$$\delta W_E = \int_{\text{Panel area}} \delta v (-\gamma_m) b_m dA \quad (2)$$

where δv is an arbitrary virtual displacement field (in the y direction), γ_m is the unit weight of the masonry panel material (the negative sign signifies that gravity acts in the negative y direction), b_m is the local thickness of the masonry panel and dA is an element of area. The integration is conducted over the area of the panel. The internal virtual work is,

$$\delta W_I = \int_{\text{Panel area}} \delta \boldsymbol{\varepsilon}^T \boldsymbol{\sigma} b_m dA + \int_0^L \delta \varepsilon_f f_f dx + \int_0^L (\delta u_f t_h + \delta v_f t_v) dx \quad (3)$$

In the first term of Eqn. (3), $\delta \boldsymbol{\varepsilon}$ and $\boldsymbol{\sigma}$ are vectors of the virtual strains and the corresponding stresses in the plane of the panel (tension positive). In the second term, $\delta \varepsilon_f$ is the virtual axial strain in the footing and f_f is the axial force in the footing. The third term in Eqn. (3) describes the soil-foundation interaction model; δu_f and δv_f are the virtual displacements (in the x and y directions respectively) of the footing and t_h and t_v are the net horizontal and vertical traction reactions applied by the soil to the footing (positive directions are indicated in Fig. 1b).

Eqns. (1-3) form the basis of a finite element representation of the S2M, formulated using a direct variational approach (see Section 2.4). The first term in Eqn. (3), relating to the panel, is formulated using conventional plane stress finite elements. The second term, relating to the strip footing, is formulated with conventional 1D bar finite elements. The third term in Eqn. (3) relates to the 1D soil-foundation interaction model, which is the key novel feature of the current paper.

2.3 1D soil-foundation interaction model

Consistent with the general approach described in Elkayam and Klar (2019), the displacements $\mathbf{u}_f = (u_f(x), v_f(x))$ induced in the idealised footing at the base of the masonry panel are considered to comprise the summation of two components:

$$\mathbf{u}_f(x) = \mathbf{u}_{\text{tun}}(x) + \mathbf{u}_{\text{def}}(x) \quad (4)$$

where $\mathbf{u}_{\text{tun}}(x) = (u_{\text{tun}}(x), v_{\text{tun}}(x))$ are the greenfield tunnel-induced ground displacements in the horizontal and vertical directions at the location of the footing and $\mathbf{u}_{\text{def}}(x) = (u_{\text{def}}(x), v_{\text{def}}(x))$ are additional traction-induced displacements caused by the action of the tractions $\mathbf{t} = (t_h(x), t_v(x))$.

The greenfield displacements $\mathbf{u}_{\text{tun}}(x)$ are treated as prescribed inputs to the problem, specified at the Gauss points in the soil-foundation interaction model. In the current analyses, greenfield displacements were determined using the 3D finite element modelling procedures in Yiu et al. (2017a), but greenfield displacements determined in other ways, e.g. using empirical approaches, could be also be employed.

The traction-induced displacements \mathbf{u}_{def} represent a modification to the greenfield displacements due to the action of soil-structure interaction mechanisms. The combined influence of the soil on the traction-induced displacements is represented in the current work by a constitutive model of the form,

$$f(t_h, t_v, u_{\text{def}}, v_{\text{def}}) = 0 \quad (5)$$

The constitutive model relates tractions and displacements at a local level, i.e. at a particular value of x ; it is therefore classified as a Winkler-type approach. Although this modelling approach excludes the spatial coupling that occurs via the soil, it does allow local frictional coupling between the horizontal and vertical tractions acting at the soil-foundation interface.

When the foundation is in compression (i.e. $v_{\text{def}} < 0$) the net vertical traction, t_v , is specified by the 2-parameter model,

$$t_v = \frac{k_v v_{\text{def}}}{1 + a_v |v_{\text{def}}|} \quad (6)$$

where k_v is the small-displacement stiffness and a_v is a parameter that governs the nonlinearity of the response. If bearing capacity failure of the soil around the footing is considered a possibility then a compression limit on t_v could be imposed, but this was not considered necessary for the current analyses.

For tension ($v_{\text{def}} > 0$) linear behaviour is assumed, $t_v = k_v v_{\text{def}}$, prior to the development of a limiting ‘uplift’ condition at large values of v_{def} . In this uplift condition, a gap forms at the base of the footing, $p_{\text{base}} = 0$, and a normal traction $p_{\text{top}} = p_t$ is imposed by the soil above the footing, where p_t is a model parameter. The limiting net vertical traction in this uplift case is $t_v = p_t + w_{\text{foot}}$. Note that this modelling approach assumes that the tensile strength of the connection between the base of the panel and the foundation exceeds the value of $p_t + w_{\text{foot}}$. The full $t_v - v_{\text{def}}$ relationship for the soil-foundation interaction model is illustrated in Fig. 2a.

An elastic-frictional model is employed for the horizontal traction, t_h (Fig. 2b). For elastic behaviour, $t_h = k_h u_{\text{def}}$, where k_h is a model parameter. Sliding occurs when the traction reaches a local limiting value, $t_h = \pm t_h^{\text{lim}}$. It is assumed that sliding initiates on all four sides of the footing at the same value of u_{def} . The local value of t_h^{lim} for incorporation in the model is therefore,

$$t_h^{\text{lim}} = \mu(p_{\text{top}} + 2p_{\text{side}} + p_{\text{base}}) \quad (7)$$

where μ is the assumed friction coefficient and p_{top} , p_{side} and p_{base} are the current values of the soil-footing normal tractions (illustrated in Fig. 1c). Although these individual normal traction components do not form an explicit part of the model, it is necessary to track them individually, as described below, to determine the current, local, value of t_h^{lim} .

To track the normal soil-footing tractions, the simple assumption is made that the side normal traction remains at its geostatic value, $p_{\text{side}} = K_0 \gamma_s (d_{\text{top}} + d_{\text{foot}}/2) d_{\text{foot}}$. For compression behaviour ($v_{\text{def}} < 0$), p_{top} remains at its geostatic value $p_{\text{top}} = \gamma_s d_{\text{top}} b_{\text{foot}}$ and the base traction is $p_{\text{base}} = \gamma_s d_{\text{base}} b_{\text{foot}} - t_v$, where t_v is the current net vertical traction. For tension (uplift) behaviour ($v_{\text{def}} > 0$), an additional assumption is needed on how the net traction t_v is apportioned between the top and bottom faces of the footing. Vertical equilibrium (neglecting any vertical shear tractions on the footing sides) requires that,

$$t_v = p_{\text{top}} + w_{\text{foot}} - p_{\text{base}} \quad (8)$$

The limiting uplift condition occurs at $p_{\text{base}} = 0$ (gap formation) and $p_{\text{top}} = p_t$ (uplift failure). It is arbitrarily assumed that the formation of a gap beneath the footing and the development of an uplift mechanism above the footing are mobilised at the same value of v_{def} . An uplift mobilisation factor, M , is therefore defined such that,

$$M = t_v / (p_t + w_{\text{foot}}) \quad (9)$$

In the geostatic state $M = 0$ and at the uplift condition, $M = 1$. At intermediate values of mobilisation, for $v_{\text{def}} > 0$, the tractions on the top and bottom of the footing are,

$$p_{\text{top}} = (1 - M)\gamma d_{\text{top}} b_{\text{foot}} + Mp_t \quad (10)$$

$$p_{\text{base}} = \gamma d_{\text{base}} b_{\text{foot}} (1 - M)$$

This gives the net vertical traction as $t_v = M(p_t + w_{\text{foot}})$ as required.

The resulting soil-foundation constitutive model is defined by five parameters $\{k_h, k_v, a_v, p_t, \mu\}$.

Procedures to estimate these parameters are discussed in Section 3.

2.4 Finite element formulation of the S2M

The model is formulated using a direct variational approach employing the weak forms in Eqns. (1-3). Conventional six-noded plane stress isoparametric triangular elements are employed for the panel and compatible three-noded Lagrangian elements are adopted for the combined footing / soil-foundation interaction model. Integration procedures are conducted numerically, via Gauss integration; three-point Gauss rules are adopted for the continuum elements and the combined footing / soil-foundation interaction elements. The soil-foundation interaction model – which is nonlinear – necessitates the use of an iterative solution strategy for the global finite element equations.

At each stage of the numerical calculation, a solution is sought to,

$$\mathbf{G} = \mathbf{F}_{\text{INT}} - \mathbf{F}_{\text{EXT}} = \mathbf{0} \quad (11)$$

where \mathbf{F}_{EXT} is the global external force vector and \mathbf{F}_{INT} is the global internal force vector. External forces occur solely due to gravity loading on the masonry panel. On the basis of the weak form in Eqn. (2), the external force vector \mathbf{f}_{EXT} , for each plane stress finite element in the panel is,

$$\mathbf{f}_{\text{EXT}} = \int_{\text{Element}} \mathbf{N}^T \mathbf{b} b_m dA \quad (12)$$

where \mathbf{N}^T is a shape function matrix, \mathbf{b} is a body force vector in which the gravity loads are specified, and the integration is conducted over the area of the element. Since the footing weight is incorporated in the initial geostatic configuration (the footing weight is exactly balanced by the geostatic soil stresses), gravity loads applied to the footing and the soil are not explicitly considered as external forces.

In the 3D finite element reference analyses, the panel is embedded within the full depth of the footing. To ensure comparability between the S2M and the reference analyses, therefore, additional gravity loads are applied to the 1D footing model in the S2M to account for the weight of the portion

of the masonry panel (of height $d_{\text{foot}}/2$) not otherwise included in the model. An additional external force component for the foundation elements is therefore determined from,

$$\mathbf{f}_{\text{EXT}} = \int_{\text{Element}} \mathbf{N}_f^T \mathbf{b}_f dx \quad (13)$$

where \mathbf{N}_f^T is a matrix containing quadratic Lagrangian shape functions and \mathbf{b}_f is a body force vector (force per unit length) corresponding to the weight of a portion of panel of height $d_{\text{foot}}/2$. (Note that in practical assessments the incorporation of \mathbf{b}_f in the model is unlikely to be needed.) The global external force vector \mathbf{F}_{EXT} is formed by assembly of the individual element vectors \mathbf{f}_{EXT} .

The internal force vector \mathbf{F}_{INT} is determined by assembling the individual contributions of the masonry panel, the footing and the soil-foundation interaction model. The internal force vectors for the panel elements are determined from,

$$\mathbf{f}_{\text{INT}} = \int_{\text{Element}} \mathbf{B}^T \boldsymbol{\sigma} b_m dA \quad (14)$$

where \mathbf{B} is a matrix containing shape function derivatives. For the footing and the soil-foundation interaction elements the combined internal force vector is,

$$\mathbf{f}_{\text{INT}} = \int_{\text{Element}} (\mathbf{B}_f^T f_f + \mathbf{N}_f^T \mathbf{t}) dx \quad (15)$$

The matrix \mathbf{B}_f is,

$$\mathbf{B}_f = [N_{1,x}(x) \quad 0 \quad N_{2,x}(x) \quad 0 \quad N_{3,x}(x) \quad 0] \quad (16)$$

where $N_{i,x}(x)$ denotes the derivative with respect to x of the quadratic Lagrangian shape functions $N_i(x)$ and \mathbf{t} is the traction vector, $\mathbf{t}^T = (t_h, t_v)$.

The S2M calculations are conducted in two stages to mimic the procedure employed in the 3D reference analyses. The model is initialised in a geostatic state with the footing (but not the panel) present. The panel is then added to the model, including gravity loading via \mathbf{F}_{EXT} , and the global nodal displacements \mathbf{U} that correspond to a solution to Eqn. (11) are determined. In a second stage, the greenfield displacements ($u_{\text{tun}}, v_{\text{tun}}$) are specified at the Gauss points of the footing / soil-foundation interaction elements; the traction-induced displacements are therefore determined as $u_{\text{def}} = u_f - u_{\text{tun}}$ and $v_{\text{def}} = v_f - v_{\text{tun}}$. Updated values of the traction vector \mathbf{t} at each Gauss point are then computed via the constitutive model in Eqn. (5) on the basis of the current traction-induced displacements. The global internal force vector is updated and a new solution to Eqn. (11) is obtained by iteration. The greenfield displacements are applied in a series of increments, with a

solution to $\mathbf{G} = \mathbf{0}$ obtained at each increment. Solutions are accepted for $\|\mathbf{G}\|_{\infty} < tol$ where tol is a specified tolerance, taken as 10 N (about half the weight of a standard house brick) in the current analyses. This value of tol was found – by numerical experimentation – to be suitable.

The adopted solution process employs a quasi Newton-Raphson approach based on the global stiffness matrix, \mathbf{K}_{init} , determined once at the start of the analysis. The matrix \mathbf{K}_{init} is evaluated by assembling the contributions of the three principal components of the model (panel, footing and soil-foundation interaction model). Element stiffness matrices for the masonry panel mesh are determined using conventional approaches for plane stress elasticity. The element stiffness matrices for the combined footing / soil-foundation interaction elements are determined from,

$$\mathbf{k}_{init} = \int_{\text{Element}} (\mathbf{B}_f^T E_f A_f \mathbf{B}_f + \mathbf{N}_f^T \mathbf{D}_s \mathbf{N}_f) dx \quad (17)$$

where E_f , A_f are the Young's modulus and cross section area, respectively, of the footing and \mathbf{D}_s is the initial constitutive matrix (i.e. for the case where the traction-induced displacements are zero) for the soil-foundation constitutive model,

$$\mathbf{D}_s = \begin{bmatrix} k_h & 0 \\ 0 & k_v \end{bmatrix} \quad (18)$$

At each stage in the solution process, an updated estimate for the nodal displacements \mathbf{U}_{k+1} based on the previous iterate \mathbf{U}_k is determined from the solution, via LU factorisation of \mathbf{K}_{init} , to,

$$\mathbf{K}_{init}(\mathbf{U}_{k+1} - \mathbf{U}_k) = \mathbf{F}_{EXT} - \mathbf{F}_{INT} \quad (19)$$

This initial stiffness procedure was found to be an efficient and stable solution process.

3.0 Calibration of the 1D soil-foundation interaction model

3.1 Calibration procedures

The soil-foundation constitutive model is defined by five parameters $(k_h, k_v, a_v, p_t, \mu)$. The parameters p_t and μ can be estimated with simple correlations and assumptions, see below, but determining k_h , k_v and a_v requires bespoke 3D finite element calibration analyses for the considered foundation and geotechnical conditions (although considerations of the building properties and tunnel excavation processes are not needed).

The models described in this paper employ the strip footing geometry from Yiu et al. (2017a) with dimensions $b_{foot} = 1$ m, $d_{base} = 1$ m and $d_{foot} = 0.5$ m (see Fig. 1c). The calibration analyses require the length of the strip footing to be defined. In the current approach a footing length of 40 m is considered, consistent with the length of the building models considered in the example analyses

in Section 4. However, the particular footing length employed in the calibration analysis is not considered to be consequential for the fidelity of the model. The Terrace gravel is represented with the Extended Mohr Coulomb model of Doherty & Wood (2013). The underlying London clay is represented with the nested yield surface model of Houlsby (1999). A selection of the adopted soil parameters is listed in Table 1; full details on the soil models and parameters are given in Yiu et al. (2017a).

Two separate 3D finite element calibration analyses are conducted for the calibrations, as illustrated in Fig. 3. Calibration A – used to evaluate k_v and a_v – comprises a plain (no openings) elastic panel with above-ground height $H = 8$ m supported on an embedded strip footing; data on thickness, unit weight and elastic parameters for the panel are listed in Table 1. An analysis is conducted in which gravity loads are applied to the panel and the vertical displacements at the base of the footing are computed. Gravity loads applied to the footing are then artificially increased by factor η and the corresponding footing displacements are determined. This analysis is, in effect, an ‘indentation test’; the relationship between the applied gravity loads and the footing displacements is used to estimate values for k_v and a_v .

Calibration B aims to estimate the lateral stiffness k_h . In this analysis, the footing alone is incorporated in the 3D finite element model (i.e. the panel is absent). Gravity loads applied to the footing are artificially increased so that the overall weight of the footing is equivalent to the weight of the combined footing and panel. An external horizontal traction, P_e , is then applied to one end face of the footing and the resulting horizontal displacements u_f of all of the nodes in the footing are computed. Values of P_e are selected to be less than the limit value that would cause frictional sliding at the soil-footing interface. The resulting displacement data are used to estimate the lateral stiffness k_h . This is achieved by matching the results of the calibration analysis with the idealised model in Fig. 3b in which the strip footing is represented as a rod being pushed through an elastic Winkler medium with horizontal traction $t_h = k_h u_f$. The displacements u_f and the internal rod axial force f_f are determined by,

$$\frac{d^2 u_f}{dx^2} - \frac{k_h u_f}{E_f A_f} = 0; \quad f_f = E_f A_f \frac{du_f}{dx} \quad (20)$$

Eqn. (20) is solved with the boundary conditions $u_f(L) = u_L$, where u_L is the displacement at $x = L$ determined from the 3D calibration analysis, and $f_f(0) = -A_f P_e$ to give,

$$u_f = \left[u_L \operatorname{sech} \alpha L + \frac{P_e}{\alpha E_f} \tanh \alpha L \right] \cosh \alpha x - \frac{P_e}{\alpha E_f} \sinh \alpha x ; \quad (21)$$

$$\alpha^2 = \frac{k_h}{E_f A_f}$$

The limiting uplift resistance p_t is determined from the correlation in Murray & Geddes (1987) for the vertical pull-out resistance of a strip anchor in sand,

$$p_t = \gamma_s (b_{\text{foot}} \times d_{\text{top}}) \left[1 + \frac{d_{\text{top}}}{b_{\text{foot}}} \tan \phi \right] \quad (22)$$

where ϕ is the soil friction angle. The friction coefficient μ is chosen to be consistent with the 3D reference analyses (Yiu et al. 2017a).

3.2 Baseline calibration data

The vertical footing displacements computed by the 3D model for the facade installation phase of Calibration A are plotted in Fig. 4a; the mean settlement is 1.74 mm. The computed variation of average net vertical line traction, t_v , and the mean displacement of all of the nodes on the base of the footing centreline, are shown in Fig. 4b. The parameters $k_v = 28.7$ MPa and $a_v = 50$ m⁻¹ were selected to provide a fit of Eqn. (6) to these data.

The Calibration B analyses were conducted by applying an external horizontal traction $P_e = 1255$ kPa in a series of load increments. This value of P_e was selected on the basis that it would cause the frictional capacity of the soil-footing interface to be approached, but not exceeded. The computed displacements u_f and axial force f_f for $P_e = 1255$ kPa, and also for a smaller value, $P_e = 628$ kPa, are plotted in Fig. 5. For each case, values of k_h have been found that provide a fit with the data when the model in Eqn. (21) is employed. This fitting process determined that $k_h = 16.9$ MPa for $P_e = 628$ kPa and $k_h = 12.3$ MPa for $P_e = 1255$ kPa. The horizontal soil stiffness therefore seems to reduce with increasing displacement. While it would be possible to incorporate this nonlinearity in the model, for simplicity a constant value of k_h is employed. The value of k_h adopted in the following example analyses is selected somewhat arbitrarily as the average of the two values specified above, i.e. $k_h = 14.6$ MPa.

The constant volume friction angle employed for the Terrace gravel in the 3D reference analyses ($\phi'_{cv} = 35^\circ$) is adopted in Eqn. (22) to give $p_t = 13.2$ kN/m. Consistent with the reference analyses, the friction coefficient is selected as $\mu = 0.3$.

These calibration parameters (referred to later as the 'baseline parameters') are listed in Table 2.

4.0 Predictive performance of the S2M

4.1 Example analyses

A set of example analyses employing the S2M with the baseline parameters in Table 2 has been conducted for the tunnel-soil-building configuration shown in Fig. 6; this configuration consists of a two-storey facade of height $H = 8$ m above ground level and length $L = 40$ m. Either a single tunnel, or a pair of tunnels, are constructed beneath the facade with eccentricity e at 5 m intervals in the range $0 < e < 25$ m. The facade is shown in Fig. 6a as having openings for windows and doors; an alternative plain facade configuration, with the same overall dimensions but without openings, is also considered. The facade is founded a strip footing, employing the geometry shown in Fig. 1c.

3D finite element reference analyses have been conducted for these example configurations using the procedures described in Yiu et al. (2017a); these analyses employed the finite element program Abaqus v2016 (Dassault Systèmes Simulia Corp., Providence, RI, USA). An example mesh is shown in Fig. 7. These reference analyses employed a linear elastic model for the masonry panel and footing (Young's modulus $E_m = 3$ GPa and Poisson's ratio $\nu_m = 0.2$); this is in contrast to the nonlinear masonry model that was employed in the analyses reported in Yiu et al. (2017a). In all other respects, however, the current 3D finite element reference analyses employ the models, procedures, dimensions and parameters specified in Yiu et al. (2017a).

The tunnel-induced greenfield ground movements specified in the S2M are obtained from prior 3D finite element results computed at the level of the base of the strip footing (although the strip footing and building were absent from the finite element model). These greenfield data are plotted in Fig. 6 of Yiu et al. (2017a), for each of the single and twin tunnel cases. In the S2M, the footing is notionally located at the mid-depth of the footing; there is therefore a small inconsistency (with the reference analyses) in the precise location at which the greenfield ground movements are applied but this is an inevitable consequence of the geometric simplifications that are employed in the S2M.

The meshes employed in the S2M analyses are shown in Fig. 8; these are closely based on the panel meshes employed in the reference analyses.

Comparisons between the tunnel-induced displacements (i.e. the incremental displacements due solely to the construction of the tunnel(s)) computed at the base of the footing from the 3D reference analyses and the footing displacements computed using the S2M are shown in Fig. 9 (for

the single tunnel case) and Fig. 10 (for the twin tunnel case) for the facade with openings. A reasonable match between the two sets of data is apparent in most cases. A similar quality of agreement between the S2M analyses and the reference analyses was found for the plain facade. Also shown in the figures, for comparison, are the greenfield settlement profiles that were specified in the S2M analyses.

Values of characteristic tensile strain, ε_{99}^t , obtained from both the S2M and the 3D reference analyses are plotted in Fig. 11. (Note that all data on characteristic strain reported in this paper refer to incremental strains due solely to the construction of the tunnel(s)). The S2M provides a close match with the corresponding 3D finite element results in most cases. The closeness of the fit is quantified by two separate metrics. In determining these metrics, the computed data are summed over a set of notional analyses comprising tunnel eccentricities at 5 m spacing in the range $-25 \text{ m} \leq e \leq 25 \text{ m}$; the notional set comprises $n = 11$ configurations. To evaluate the metrics, computed data for negative values of tunnel eccentricity are identical (due to symmetry) to the corresponding positive value.

The root mean squared (RMS) difference Δ^{RMS} is defined,

$$\Delta^{\text{RMS}} = \sqrt{\frac{1}{n} \sum_{e=-25\text{m}}^{e=25\text{m}} \left(\frac{[\varepsilon_{99}^t]_e^{\text{S2M}} - [\varepsilon_{99}^t]_e^{\text{FE}}}{[\varepsilon_{99}^t]_e^{\text{FE}}} \right)^2} \quad (23)$$

where $[\varepsilon_{99}^t]_e^{\text{FE}}$ and $[\varepsilon_{99}^t]_e^{\text{S2M}}$ are values of characteristic strain determined from the 3D finite element reference analyses and the S2M, respectively, for a tunnel eccentricity e . The RMS difference metric provides an indication of the closeness of fit of the S2M to the finite element data but it does not indicate whether any systematic bias exists. A separate parameter Δ^{Diff} is therefore defined,

$$\Delta^{\text{Diff}} = \frac{1}{n} \sum_{e=-25\text{m}}^{e=25\text{m}} \frac{[\varepsilon_{99}^t]_e^{\text{S2M}} - [\varepsilon_{99}^t]_e^{\text{FE}}}{[\varepsilon_{99}^t]_e^{\text{FE}}} \quad (24)$$

Positive values of Δ^{Diff} indicate that the S2M values of characteristic strain systematically exceed the corresponding finite element data (and vice versa for negative values of Δ^{Diff}).

Values of these metrics are listed in Table 3. In all cases – as expected from visual inspection of Fig. 11 – all values of Δ^{Diff} are positive, indicating that the characteristic strain from the S2M results systematically exceeds the corresponding reference data. Values of Δ^{RMS} all lie in the region $11.3\% \leq \Delta^{\text{RMS}} \leq 17.7\%$. Although these values of Δ^{RMS} indicate that the S2M is subject to some

loss of fidelity – compared with the corresponding finite element analysis – the multiple uncertainties in other aspects of the problem in practical assessment scenarios are likely to mean that fidelity losses of this magnitude in the 1D soil-foundation model will have limited practical significance. This issue is further discussed in Section 6.

4.2 Demonstration case

A separate, demonstration case (Fig. 12) has been developed to demonstrate the performance of the S2M for a facade that differs significantly from the example analyses above, although employing the same foundation details and geotechnical conditions. The facade employed in this case applies rather more gravity loading to the foundation than the facade in the previous example analyses.

The building details employed in the demonstration case are based on those in Giardina et al. (2013) (with the facade of total length 14.28 m in Giardina et al. (2013) repeated and adjusted in the current model to give a facade of length 29m). The wall thickness was 0.25 m and the Young's modulus of the masonry and the footing was $E = 1$ GPa; these values were selected to ensure that a building response intermediate between stiff and flexible would develop. All other parameters employed in the analyses are listed in Table 1. The tunnelling configuration is based on data in Withers (2001) that relate to the construction of the Jubilee Line extension in London.

Greenfield foundation-level ground movements were determined using the procedures in Yiu et al. (2017a) on the basis that both tunnels are constructed simultaneously. A fully coupled tunnel-soil-building 3D finite element analysis was also conducted, employing a linear elastic model for the façade. Separately, the computed greenfield movements were specified as input parameters to the S2M to obtain an independent prediction. Computed tunnel-induced settlements are compared in Fig. 13; a reasonable match appears to have been achieved. The computed value of ε_{99}^t from the S2M was $103 \mu\epsilon$; a value of $\varepsilon_{99}^t = 103 \mu\epsilon$ was also obtained from the 3D finite element analysis.

5.0 Sensitivity analyses

In practical damage assessment activities, there are invariably significant uncertainties around the local ground conditions and the geometrical and mechanical characteristics of a building's foundations. To inform the selection of parameters for the 1D soil-foundation interaction model, it is instructive to consider the influence that variations in the input parameters have on the predicted level of damage. A sensitivity study has therefore been conducted as described below.

The influence of varying the individual model parameters (with respect to the baseline parameters in Table 2) is quantified by the variation metric Δ^{Var} ,

$$\Delta^{\text{Var}} = \frac{1}{n} \sum_{e=-25m}^{e=25m} \frac{[\overline{\varepsilon_{99}^t}]_e^{\text{S2M}} - [\varepsilon_{99}^t]_e^{\text{S2M}}}{[\varepsilon_{99}^t]_e^{\text{S2M}}} \quad (25)$$

where $[\overline{\varepsilon_{99}^t}]_e^{\text{S2M}}$ is the value of ε_{99}^t determined via the S2M, employing a single modified parameter and $[\varepsilon_{99}^t]_e^{\text{S2M}}$ is the corresponding value obtained with the baseline parameters. The summation is conducted over $n = 11$ values of tunnel eccentricity at 5 m spacings in the range $-25 \text{ m} \leq e \leq 25 \text{ m}$. The overbar convention employed in Eqn. (25) to indicate a modified parameter is adopted in the following text. Results for the computed variation metrics are listed in Table 4.

5.1 Vertical stiffness, k_v

In practical cases it is inevitable that significant uncertainties will exist around appropriate parameters to define the vertical stiffness of the foundation. For example, the stiffness characteristics of sand and gravel materials will be influenced by the magnitude of the local compressive stresses. Beneath a building foundation the stresses are locally increased by the weight of the building; the incremental stiffness of the foundation – relevant to its response to tunnel-induced movements – will therefore be difficult to quantify. Similar questions will exist for buildings founded on clay soils. The parameter, k_v is likely to have a dominant influence in determining the overall soil-structure interaction behaviour in most cases. Understanding the influence of k_v on the performance of the model is therefore of prime importance.

Two separate sets of sensitivity analyses have been conducted using modified parameters $\bar{k}_v = 2k_v$ and $\bar{k}_v = k_v/2$ where k_v is the baseline value in Table 2. The results in Table 4 indicate that variations in k_v have a significant influence on the computed characteristic strains. Increasing k_v tends to cause ε_{99}^t to increase (positive values of Δ^{Var}); stiffer soil would be expected to induce increased deformations in a building and so this observed behaviour is as expected. Similarly, when k_v is reduced the values of ε_{99}^t also reduce (negative values of Δ^{Var}).

5.2 Horizontal stiffness, k_h

Consistent with the sensitivity studies on k_v , analyses have been conducted with $\bar{k}_h = 2k_h$ and $\bar{k}_h = k_h/2$. In all cases the predicted values of ε_{99}^t were found to be insensitive to variations in k_h . It appears that, in these analyses, the horizontal soil-foundation interaction is dominated by frictional sliding and so the elastic stiffness is relatively unimportant.

A separate investigation on the significance of the horizontal stiffness for the computed characteristic strain for the demonstration case in Section 4.2 indicated that for $\bar{k}_h = 2k_h$ and $\bar{k}_h = k_h/2$ the computed characteristic strain was increased by 3% and reduced by 6%, respectively, with respect to the baseline values. This case is therefore rather more sensitive to k_h than the example analyses; this is presumably due to the fact that, in the demonstration case, the horizontal tunnel-induced greenfield displacements are relatively small and so more of the soil-footing interface is elastic.

5.3 Friction coefficient, μ

Calculations have been conducted in which μ is separately set to zero (smooth interface) and to $\mu = \tan \phi'_{cv}$ (fully rough interface) where $\phi'_{cv} = 35^\circ$ is the constant volume friction angle for the soil employed in the 3D reference analyses. The results of this study indicate a pattern of behaviour in which the influence of varying the friction coefficient differs depending on whether the plain facade or the facade with openings is considered.

For the facade with openings, the computed characteristic strains reduce slightly when the friction coefficient is set to zero and increase when the interface is made fully rough, compared with the baseline case. This closely mimics the results obtained in separate 3D finite element calculations by Yiu et al. (2018) – for the same facade with openings configuration that is considered here (but with a nonlinear masonry model) – in which increasing the soil-footing interface friction coefficient from zero to a fully rough case was found to cause the computed value of ε_{99}^t to increase systematically. There appear to be two competing mechanisms at play; increasing the friction coefficient is found in the current results (and in Yiu et al. 2018) to have the beneficial effect of reducing the differential settlements across the building, implying reduced damage. Conversely, the additional strains induced in the building – due to horizontal base tractions for nonzero values of friction coefficient – appear to have a detrimental effect, causing the computed characteristic strains to increase. For the facade with openings, the detrimental horizontal base traction mechanism seems to slightly outweigh the beneficial effect of the reduction in differential settlement.

In the plain facade case, the influence of friction coefficient on ε_{99}^t follows a different pattern. In this case the smooth interface analyses predict values of ε_{99}^t that are substantially greater than the baseline case. The computed magnitudes of ε_{99}^t tend to reduce as μ is increased.

These results illustrate the necessity of incorporating a realistic soil-foundation interface friction model within assessment analyses. This is especially important for applications where the ground movements imposed on the building are sufficiently large that slipping occurs at the soil-foundation interface, as in the current example.

5.4 Limiting uplift resistance, p_t

The parameter p_t might initially seem to be a relatively minor component of the model. However, the modelling results demonstrate that, in some cases, variations in p_t can have a significant influence on the computed value of ε_{99}^t . In particular, in the current example analyses the combined effect of relatively large ground movements and a relatively stiff building means that in some cases the model predicts that ‘gaps’ will form beneath the footing; the presence of gaps, in turn, influences the magnitude and distribution of induced strains within the facade. This gapping phenomenon has been previously observed by other researchers, e.g. in the centrifuge tests reported in Ritter (2018). The tendency of gaps to occur is influenced by the value of p_t adopted in the model.

Separate numerical experiments have therefore been conducted in which (i) p_t is increased to a sufficiently large value to ensure that a limiting uplift condition does not occur, and (ii) a no-tension condition is imposed at the base of the panel. The results in Table 4 indicate that increasing the limiting uplift resistance to a large value can have a significant detrimental effect on the computed characteristic strain due to the closing of gaps; this is especially the case for the plain facade case. With a no-tension condition applied at the base of the panel, the computed values of characteristic strain are, in all cases, significantly less than the baseline values.

6.0 Discussion

Values of characteristic tensile strain ε_{99}^t computed for all of the models considered in this paper are relatively low, compared with the tensile strain magnitudes that are typically considered to be of concern in practical assessments. For the example analyses using the facade with openings, Fig. 11, the characteristic strain is in most cases less than $500 \mu\varepsilon$. According to the widely-used strain-based damage criteria (e.g. Mair et al. 1996) this would place the majority of these cases in damage category ‘negligible’. These relatively low values of characteristic strain are attributable to the simplified building model – employing elastic behaviour – that has been adopted in the S2M to demonstrate the 1D soil-foundation model. Results in Yiu et al. (2017a) demonstrate that the

incorporation of masonry nonlinearity in the structural model causes significantly larger characteristic tensile strains to develop than those reported here. The 1D soil-foundation model can readily be combined with more realistic structural models, e.g. incorporating nonlinear material behaviour, although this extension is beyond the current scope.

The current implementation of the S2M required about 3 minutes to compute each of the example analyses using a standard laptop computer, without any special efforts to accelerate the calculation. In contrast, the corresponding 3D finite element analyses required several hours of CPU time, in addition to the considerable work that is required to set up each analysis. The general framework developed for the S2M therefore seems a suitable basis for practical assessment exercises for which a large number of rapid, robust, computations are required.

The fidelity with which the S2M is able to match the damage metric predictions obtained by detailed 3D finite element analyses is considered reasonable in most cases – given the relative simplicity of the model; it is therefore considered suitable for use in routine damage assessment procedures. But significant differences between the S2M results and the corresponding 3D finite element results do exist in some cases. Investigations have been conducted as follows to determine the sources of these fidelity losses in the 1D soil-foundation model.

First, the installation of tunnel(s) in the 3D finite element reference analyses induces significant adjustments to the stresses and strains in the ground in the neighbourhood of the footing. For example, in the greenfield case, horizontal strains of the order of $\pm 0.2\%$ develop at the level of the foundation for the single and twin tunnel cases (see Fig. 6 of Yiu et al. 2017a). These tunnel-induced strains have been shown in exploratory calculations (not reported here) to have a significant influence on the incremental response of the building. The values of k_v and a_v determined with Calibration A, in which the tunnel is absent from the model, do not account for this mechanism. A process has been devised (not reported here) in which the 1D soil-foundation interaction model is extended to encompass this effect by incorporating an additional model parameter and employing an additional 3D finite element calibration analysis in which the influence of tunnel-induced soil disturbance around the footing is addressed. This process leads to a softer response (lower value of k_v) in the regions where high lateral tunnel-induced tensile strains develop in the soil. Although this extended S2M provides some improvement to the fidelity of the model, compared with the 3D reference analyses, the additional complexity of the extended model is not considered to be justified by the modest improvement in performance. It is considered, however, that this mechanism – in

which tunnel-induced strains in the soil act to modify the incremental soil response around the foundation – may be a significant factor in some tunnel-soil-building interaction scenarios.

Second, the adoption of an elasto-plastic model to represent the Terrace gravel in the 3D finite element reference analyses allows for the possibility of horizontal tractions applied to the soil beneath the footing causing the occurrence of additional vertical displacements. This horizontal-vertical plastic coupling effect has been proposed by Elkayam and Klar (2019) to have an influence on the computed structural displacements in tunnel-soil-building analyses that are broadly comparable to those presented in the current paper. This elasto-plastic coupling mechanism – which is absent from the S2M but implicit in the 3D reference analyses– may explain some of the differences between the S2M and the 3D finite element reference analyses in Figs 9 and 10.

Third, the modelling errors implicit in the Winkler approach, in which spatial coupling in the soil is not considered, will result in some loss of fidelity. A separate implementation of the 1D soil-foundation interaction model was developed using a Pasternak model, in which spatial coupling within the soil can be approximately represented. However, the additional work involved in selecting and calibrating appropriate nonlinear models for the shear coupling component of the Pasternak model appeared to be unduly onerous when balanced against the likely improvements in performance. Separately, however, it was found that the fidelity of the Winkler model incorporated in the 1D soil-foundation interaction model could be significantly improved by ‘tuning’ the model parameters to obtain an optimum match with a subset of the 3D reference analyses (selected in these investigations to be the zero tunnel eccentricity cases). This tuning process involves adjusting the coefficients in the Winkler model to partially ‘calibrate out’ the modelling errors. Such an approach has been found to be useful in other applications of Winkler-type models for soil-foundation interaction (Burd et al. 2020). In the current application, however, the uncertainties in the characteristics of the buildings and foundations encountered in practical assessment projects are thought likely to outweigh significantly the modelling errors implicit in the Winkler approach. The adoption of ‘tuned’ models is therefore not proposed in the current work.

The reported sensitivity study indicates that, for the particular analysis conditions being considered, damage predictions from the S2M are strongly influenced by certain of the parameters, particularly k_v , μ and p_t . The strong observed dependency on k_v suggests that the additional overhead in conducting finite element-based calibration procedures to determine this particular parameter is likely to be justified in practical applications of the approach. It is possible – although this has not yet

been tried – that k_v and α_v could be determined more straightforwardly by using a 2D plane strain finite element analysis for the calibration calculation, rather than the 3D analysis used here.

Conversely, the relatively weak dependency of the computed characteristic strain on the horizontal stiffness k_h suggests that simpler approaches to estimate this parameter, as an alternative to a bespoke finite element calibration analysis as employed here, might be appropriate.

Accurate values of the friction coefficient, μ , are unlikely to be known with certainty in any practical case, and in practical assessments it is suggested that a range of plausible values of μ be considered, with the most onerous case taken as the governing condition. Such an approach is facilitated by the relatively low computational cost of the S2M.

The limiting uplift resistance parameter p_t can be estimated using existing geotechnical correlations. Increasing the value of p_t is seen to increase the level of predicted damage. In practical assessments it may be appropriate to assume the largest plausible value of p_t on the basis that this is likely to lead to a conservative result. However, the transmission of uplift resistance to the building requires the development of tensile stresses at the base of the panel. If the bed joint at the base of the panel is unable to sustain significant tension then the influence of the uplift resistance on the settlement-induced damage may be reduced. Paradoxically a weak bed joint at the base of a masonry wall or facade may act to reduce the extent of damage elsewhere in the wall or facade.

7.0 Conclusions

A simplified 1D model to represent the strip footing and various soil-foundation interaction mechanisms has been developed for the purpose of conducting rapid damage assessments for masonry buildings affected by tunnelling. The model has been demonstrated by coupling it with a 2D finite element model of a masonry facade. This semi-coupled model possesses a level of sophistication that allows it to mimic predictions of tunnel-induced damage (via the characteristic strain parameter ε_{99}^t) obtained from detailed 3D finite element analyses, following an initial calibration of the model parameters via relatively straightforward procedures.

Calibration of the soil-foundation interaction model employs bespoke 3D finite element analyses to determine the values of parameters that define the horizontal and vertical stiffness. The calibration is demonstrated for geotechnical conditions that are considered to be representative of London, but the same approach is applicable to other soil conditions provided that sufficient geotechnical data

are available to calibrate a plausible finite element model. It is clear that successful application of the model in a field context would require appropriate geotechnical characterisation of the site to support the calibration process and the estimation of the greenfield ground movements.

Funding sources

This research did not receive any specific grant from funding agencies in the public, commercial, or not-for-profit sectors.

Nomenclature

a_v	Nonlinear response parameter in soil-foundation interaction model
b_{foot}	Width of the footing
b_m	Thickness of the masonry panel
d_{base}	Depth of the base of the footing beneath the ground surface
d_{foot}	Thickness of the footing
d_{top}	Depth of the top of the footing beneath the ground surface
k_v	Small-displacement vertical stiffness parameter in soil-foundation interaction model
k_h	Horizontal stiffness parameter in soil-foundation interaction model
\mathbf{t}	Traction vector, $\mathbf{t}^T = (t_h, t_v)$
p_{base}	Normal traction (force per unit length) at the base of the footing
p_t	Limiting uplift parameter (force per unit length) in soil-foundation interaction model
p_{top}	Normal traction (force per unit length) at the top of the footing
p_{side}	Normal traction (force per unit length) at the sides of the footing
t_h	Net horizontal traction (force per unit length) at soil-footing interface
t_h^{lim}	Limiting net horizontal traction (force per unit length) at soil-footing interface
t_v	Net vertical traction (force per unit length) at soil-footing interface
\mathbf{u}_{def}	Vector of traction-induced ground displacements in the x and y directions, $\mathbf{u}_{\text{def}} = [u_{\text{def}}, v_{\text{def}}]$, at the location of the idealised footing
\mathbf{u}_f	Vector of footing displacements in the x and y directions, $\mathbf{u}_f = [u_f, v_f]$
\mathbf{u}_{tun}	Vector of prescribed greenfield tunnel-induced ground displacements in the x and y directions, $\mathbf{u}_{\text{tun}} = (u_{\text{tun}}, v_{\text{tun}})$, at the location of the idealised footing
w_{foot}	Footing weight (force per unit length)
H	Height of masonry panel above the ground surface
K_0	Coefficient of lateral earth pressure
M	Uplift mobilisation factor
ε_{99}^t	Characteristic strain; the lowest value of tunnel-induced tensile strain that is not exceeded in 99% of the facade area
μ	Coefficient of friction at the soil-footing interface
ϕ	Soil friction angle
ϕ'_{cv}	Soil friction angle at constant volume
γ_m	Unit weight of masonry
γ_s	Unit weight of the Terrace gravel

Δ^{Diff}	Metric describing the average difference in characteristic strain values computed using the S2M and the 3D finite element reference analyses
Δ^{RMS}	Metric describing the RMS difference between characteristic strain values computed using the S2M and the 3D finite element reference analyses
Δ^{Var}	Metric describing the average change in characteristic strain values, computed using the S2M, due to an adjustment of a parameter from its calibrated value

References

- Acikgoz, S., Franza, A., DeJong, M. J., & Mair, R. (2021). Cracked Equivalent Beam Models for Assessing Tunneling-Induced Damage in Masonry Buildings. *Journal of Geotechnical and Geoenvironmental Engineering*, 147(2).
- Addenbrooke, T. I. & Potts, D. M. (2001). Twin tunnel interaction: surface and subsurface effects. *International Journal of Geomechanics*, 1(2), 249-271.
- Basmaji, B., Deck, O. & Al Heib, M. (2019). Analytical model to predict building deflections induced by ground movements. *European Journal of Environmental and Civil Engineering*, 23(3), 409-431.
- Burd, H.J., Taborda, D.M.G. Zdravković, L. Abadie, C.N., Byrne, B.W., Houlsby, G.T., Gavin, K.G., Igoe, D.J.P., Jardine, R.J., Martin, C.M., McAdam, R.A., Pedro, A.M.G. & Potts, D.M. (2020). PISA design model for monopiles for offshore wind turbines: application to a marine sand. *Geotechnique*, 70(11), 1048-1066.
- Burland J.B. (2001). Assessment methods used in design. In *Building response to tunnelling: case studies from construction of the Jubilee Line Extension, London, volume 1: the project* (eds J. B. Burland, J. R. Standing and F. M. Jardine), 23–43.
- Burland, J. B. & Wroth, C. P. (1974). Settlement of buildings and associated damage. In *Proceedings of the conference on settlement of structures* (ed. A. C. Meigh), 611–654. London, UK: Pentech Press.
- Boscardin, M. D. & Cording, E. J. (1989). Building response to excavation-induced settlement. *Journal of Geotechnical Engineering*, 115(1), 1–21.
- Camós, C., Molins, C. and Arnau, O. (2014). Case study of damage on masonry buildings produced by tunneling induced settlements. *Int. J. of Architectural Heritage*, 8(4), 602-625.
- Dalgic, K. D., Hendriks, M. A., Ilki, A. & Broere, W. (2018). A two-stage numerical analysis approach for the assessment of the settlement response of the pre-damaged historic Hoca Pasha Mosque. *International Journal of Architectural Heritage*.
- Deck, O., & Singh, A. (2012). Analytical model for the prediction of building deflections induced by ground movements. *International Journal for Numerical and Analytical Methods in Geomechanics*, 36(1), 62-84.
- Divall S., Goodey R. & Taylor R. (2012) Ground movements generated by sequential twin-tunnelling in over-consolidated clay. 2nd European Conference on Physical Modelling in Geotechnics, Delft, The Netherlands.
- Doherty, J. P. & Muir Wood, D. (2013). An extended Mohr–Coulomb (EMC) model for predicting the settlement of shallow foundations on sand. *Géotechnique* 63(8), 661–673.
- Elkayam, I., & Klar, A. (2019) Nonlinear elastoplastic formulation for tunneling effects on superstructures. *Canadian Geotechnical Journal*, 56(7), 956-969.

- 749 Franza, A., & DeJong, M. J. (2019). Elastoplastic solutions to predict tunneling-induced load
750 redistribution and deformation of surface structures. *Journal of Geotechnical and Geoenvironmental*
751 *Engineering*, 145(4), 04019007.
- 752 Giardina, G., Van de Graaf, A. V., Hendriks, M. A., Rots, J. G. & Marini, A. (2013). Numerical analysis
753 of a masonry facade subject to tunnelling-induced settlements. *Engineering Structures* 54, 234-247.
- 754 Houlsby, G. T. (1999). A model for the variable stiffness of undrained clay. In *Pre-failure deformation*
755 *characteristics of geomaterials* (eds M. Jamiolkowski, R. Lancellotta and D. Lo Presti), Balkema
756 Rotterdam, the Netherlands, 1, 443–450.
- 757 Losacco, N., Burghignoli, A. & Callisto, L. (2014). Uncoupled evaluation of the structural damage
758 induced by tunnelling. *Géotechnique*, 64(8), 646-656.
- 759 Mair, R. J., Taylor, R. N. & Burland, J. B. (1996). Predictions of ground movements and assessment of
760 risk of building damage due to bored tunnelling. In *Proceedings of Geotechnical Aspects of*
761 *Underground Construction in Soft Ground* (eds R.J. Mair and R.N. Taylor), 713-718.
- 762 Mair, R.J. & Taylor, R.N. (1997). Bored tunnelling in the urban environment. In *Proceedings of the*
763 *Fourteenth International Conference on Soil Mechanics and Foundation Engineering*. Balkema,
764 Hamburg. 2353–2385.
- 765 Murray, E. J. & Geddes, J. D. (1987). Uplift of anchor plates in sand. *Journal of Geotechnical*
766 *Engineering*, 113(3), 202-215.
- 767 Ocak, I. (2014). A new approach for estimating the transverse surface settlement curve for twin
768 tunnels in shallow and soft soils. *Environmental Earth Sciences*, 1-11.
- 769 Peck, R.B., 1969. Deep excavation and tunneling in soft ground. In: *Proceedings of the International*
770 *Conference in Soil Mechanics and Foundation Engineering*, Mexico City, 225–290.
- 771 Pickhaver, J.A., Burd, H.J., & Houlsby, G.T. (2010). An equivalent beam method to model masonry
772 buildings in 3D finite element analysis. *Computers and Structures*, 88 (19-20), 1049-1063.
- 773 Rankin, W.J. (1988) Ground movements resulting from urban tunnelling: Predictions and effects.
774 Geological Society Engineering Geology Special Publication, 79-92.
- 775 Ritter, S. (2018). Experiments in tunnel-soil-structure interaction. PhD dissertation, University of
776 Cambridge.
- 777 Yiu, W. N., Burd, H. J. & Martin, C. M. (2017a). Finite-element modelling for the assessment of
778 tunnel-induced damage to a masonry building. *Géotechnique*, 67(9), 780-794.
- 779 Yiu, W. N., Burd, H. J. & Martin, C. M. (2017b). Soil–building interaction in finite element analysis of
780 tunnelling-induced building damage. In *Proceedings of the IV international conference on*
781 *computational methods in tunneling and subsurface engineering* (eds G. Hofstetter, K. Bergmeister,
782 J. Eberhardsteiner, G. Meschke and H. F. Schweiger), Innsbruck, Austria: University of Innsbruck.
783 381–388.
- 784 Yiu, W. N., Burd, H. J. & Martin, C. M. (2018). Soil-foundation contact models in finite element
785 analysis of tunnelling-induced building damage. In *Numerical Methods in Geotechnical Engineering*
786 *IX*, 2, 989-997, CRC Press.
- 787 Withers, A. D. (2001). Murdoch, Neptune and Clegg Houses in Moodkee Street, Rotherhithe. In
788 *Building response to tunnelling: case studies from construction of the Jubilee Line Extension, volume*
789 *2: case studies* (eds J. B. Burland, J. R. Standing and F. M. Jardine), 811–828. London, UK: Thomas
790 Telford.

	Parameter	Value
Masonry panel	Masonry unit weight, γ_m	23.75 kN/m ³
	Masonry panel thickness, b_m	0.215 m
	Masonry Young's modulus, E_m	3 GPa
	Masonry Poisson's ratio, ν_m	0.2
Footing	Footing Young's modulus, E_f	3 GPa
Terrace gravel	Terrace gravel unit weight, γ_s	19.5 kN/m ³
	Coefficient of lateral earth pressure, K_0	0.425
	Constant volume friction angle, ϕ'_{cv}	35°
Tunnel	Diameter	11.0 m
	Tunnel volume loss	1.5%

Table 1; Parameters adopted for the calibration analyses described in Section 3, and the example and reference analyses described in Section 4.1. Further detail on the parameters employed in the geotechnical constitutive models in the reference analyses is provided in Yiu et al. (2017a).

Parameter	Value
Horizontal stiffness, k_h	14.6 MPa
Vertical stiffness, k_v	28.7 MPa
Softening parameter, a_v	50 m ⁻¹
Limiting uplift resistance, p_t	13.2 kN/m
Soil-footing interface coefficient, μ	0.3

Table 2; Baseline calibration parameters for the 1D soil-foundation interaction model

Facade type	No. of tunnels	Δ^{RMS} (%)	Δ^{Diff} (%)
Plain	1	17.7	9.9
	2	11.3	7.5
With openings	1	14.7	9.8
	2	16.5	13.3

Table 3; Comparison metrics for the example calculations

Parameter	Modified parameter	Δ^{Var} (%); facade with openings		Δ^{Var} (%); plain facade	
		T1	T2	T1	T2
Vertical stiffness, k_v	$\bar{k}_v = 2k_v$	13.7	11.2	15.5	14.0
	$\bar{k}_v = k_v/2$	-21.8	-20.1	-29.0	-25.5
Horizontal stiffness, k_h	$\bar{k}_h = 2k_h$	0.0	0.0	0.0	0.0
	$\bar{k}_h = k_h/2$	0.0	0.0	0.1	0.1
Shear coefficient, μ	$\mu = 0$	-2.7	-1.0	10.4	14.8
	$\mu = \tan 35^\circ$	4.9	2.9	-3.8	-4.5
Limiting uplift resistance, p_t	No tension allowed at base of panel	-15.8	-21.3	-17.6	-22.6
	No limit on uplift resistance	8.2	12.9	19.2	29.5

Table 4; Variation metrics Δ^{Var} for the sensitivity study. 'T1' refers to single tunnel; 'T2' refers to twin tunnels

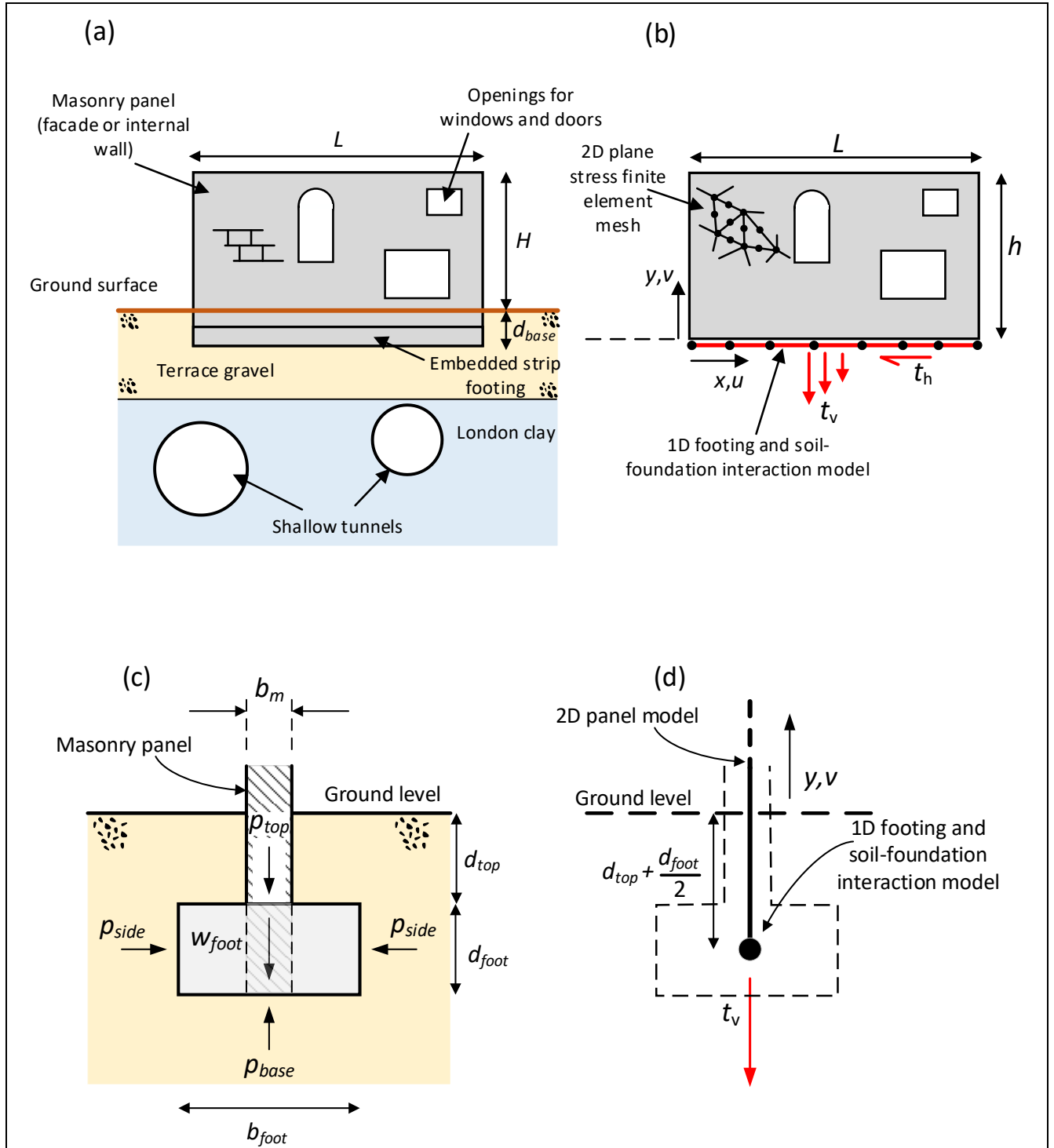
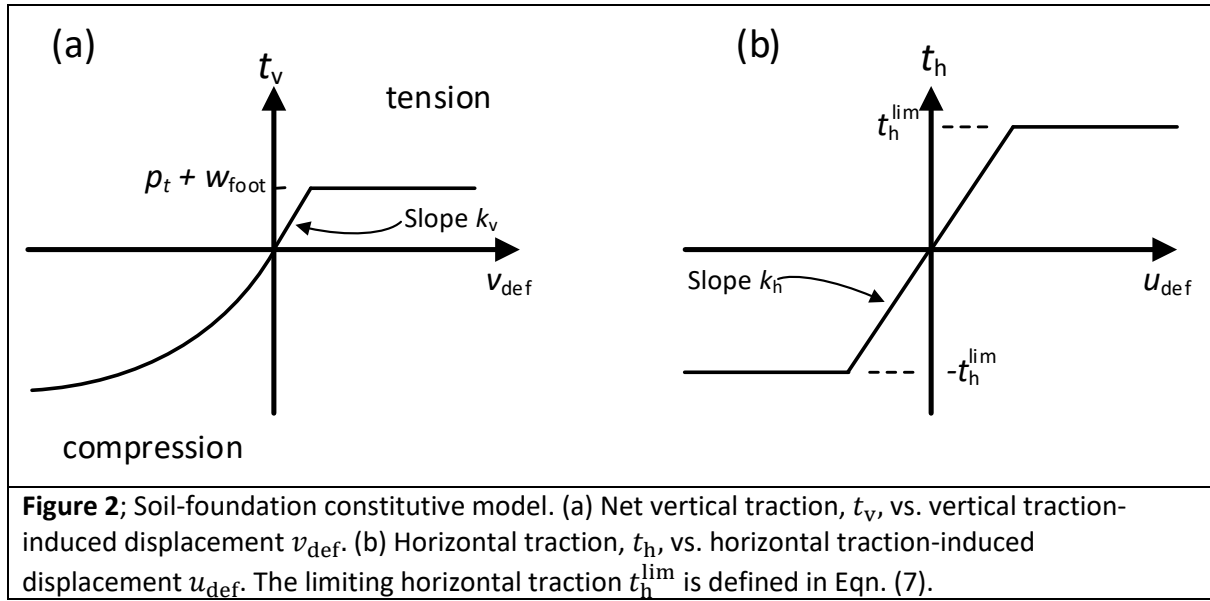
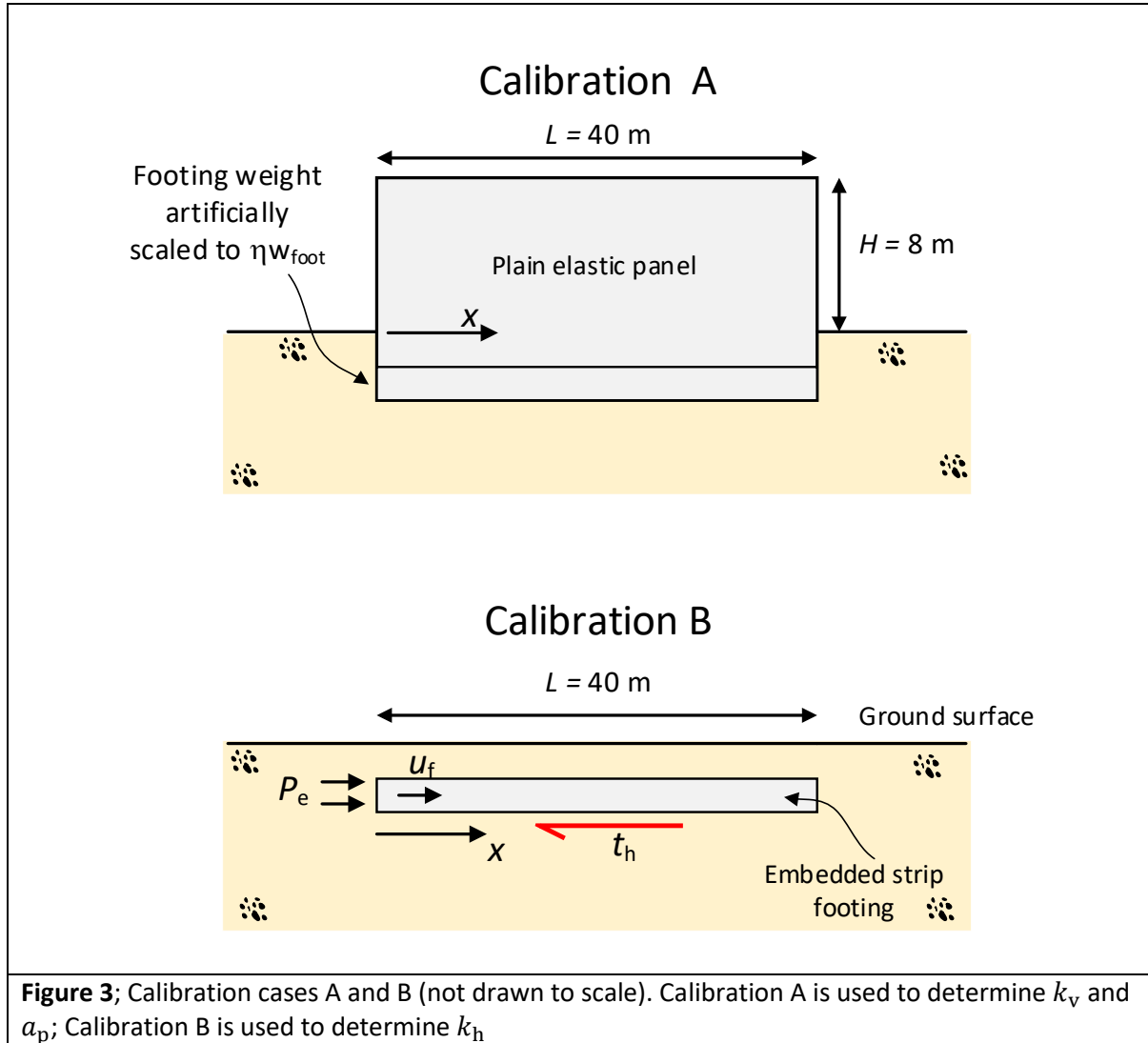


Figure 1; Basic features of the S2M. (a) Idealised form of the problem being considered. (b) General form of the S2M. The plane stress finite element mesh employed to model the masonry panel is assigned thickness b_m . The net horizontal and vertical traction reactions t_h and t_v (units force per length) are applied by the soil onto the foundation; positive directions are those shown in the figure (c) Cross section through the strip footing showing the normal line tractions p_{top} , p_{side} and p_{base} acting on the top, sides and base of the footing respectively. (d) Cross section through the S2M showing the 2D panel model and the 1D soil-foundation interaction model.





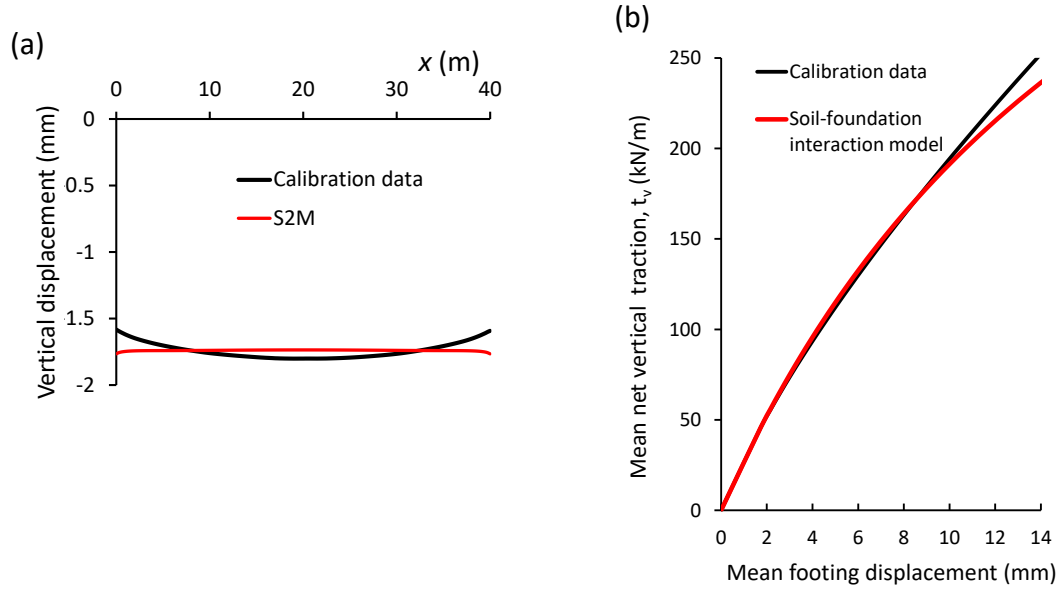


Figure 4; Results from Calibration A. 'Calibration data' refers to data from the 3D calibration analyses; 'S2M' refers to corresponding results obtained from the calibrated S2M. (a) Footing displacement due to the addition of the building to the model. (b) Average footing displacement at increased values of normal traction (displacement values are plotted as positive, for clarity).

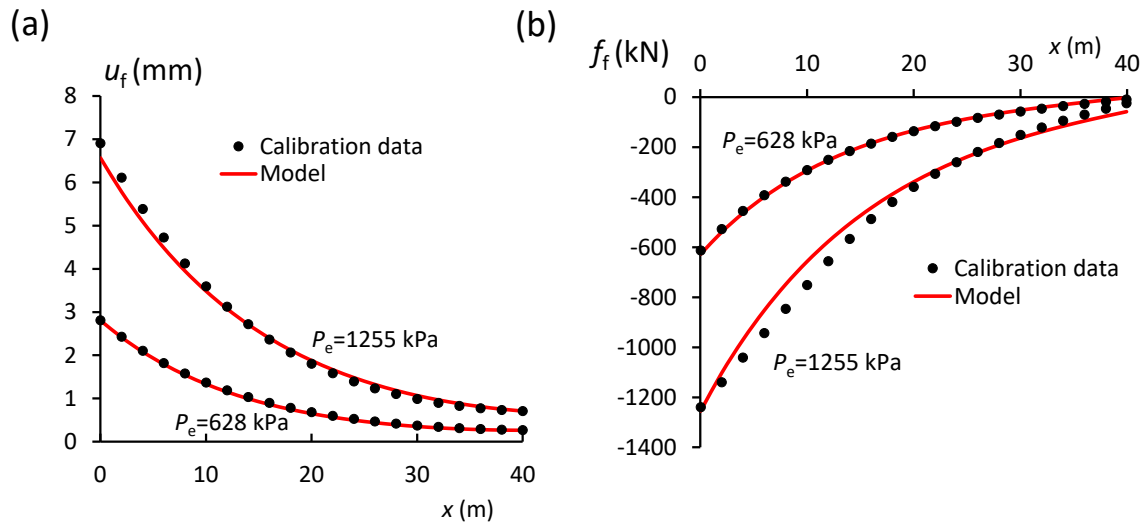


Figure 5; Results from Calibration B for applied normal end traction $P_e = 628$ kPa and $P_e = 1255$ kPa. 'Calibration data' refers to data from the 3D calibration analyses; 'Model' refers to best fit data from the model in Eqns. 20 and 21 with $k_h = 16.9$ MPa for $P_e = 628$ kPa and $k_h = 12.3$ MPa for $P_e = 1255$ kPa. (a) Footing displacements, u_f . (b) Axial force in footing, f_f .

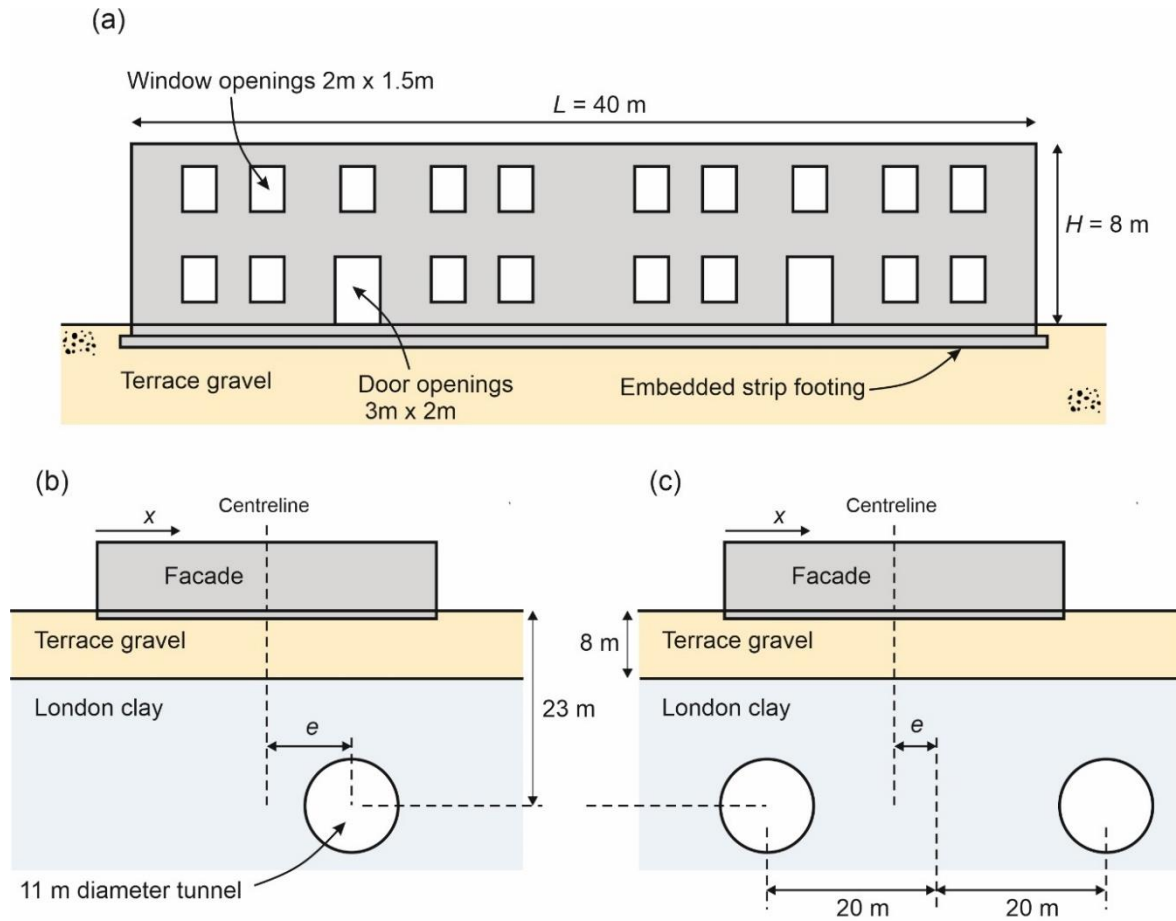


Figure 6; Reference tunnel-soil-building scenario (Yiu et al. 2017a). (a) Facade elevation; the strip footing dimensions are $d_{top} = 0.5$ m; $d_{foot} = 0.5$ m; $b_{foot} = 1.0$ m. (b) and (c) Single and twin tunnel arrangements.

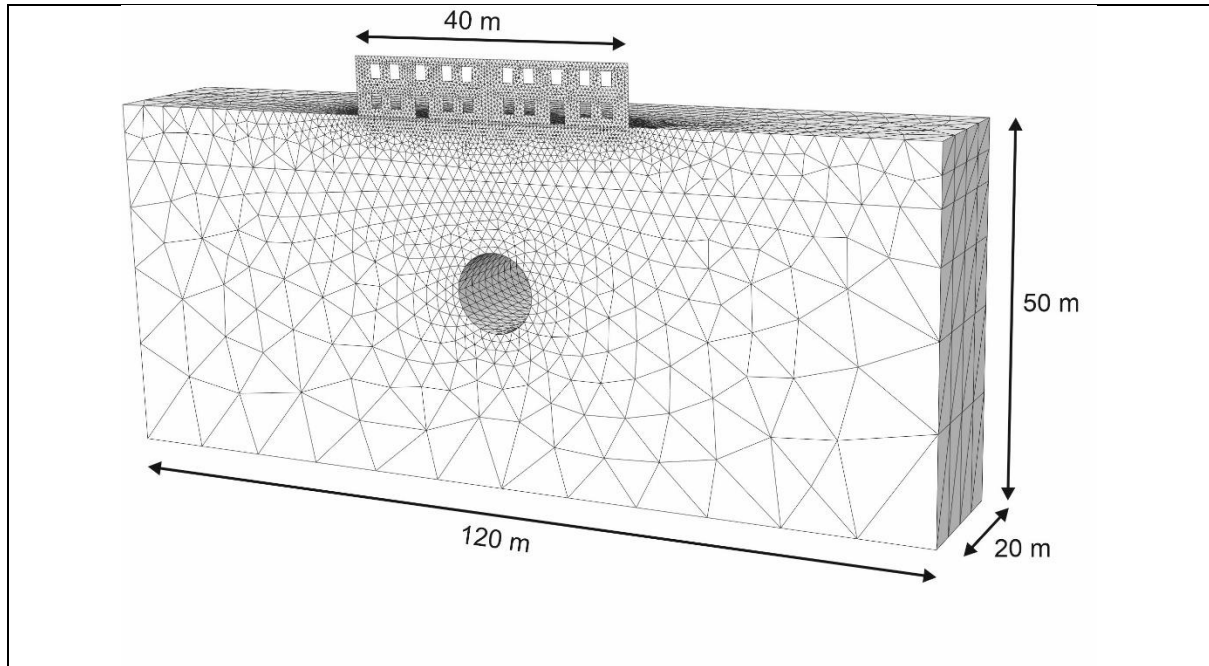


Figure 7; Finite element mesh (reproduced from Yiu et al. 2017a) employed in the 3D finite element reference analysis of a single zero-eccentricity tunnel.

833

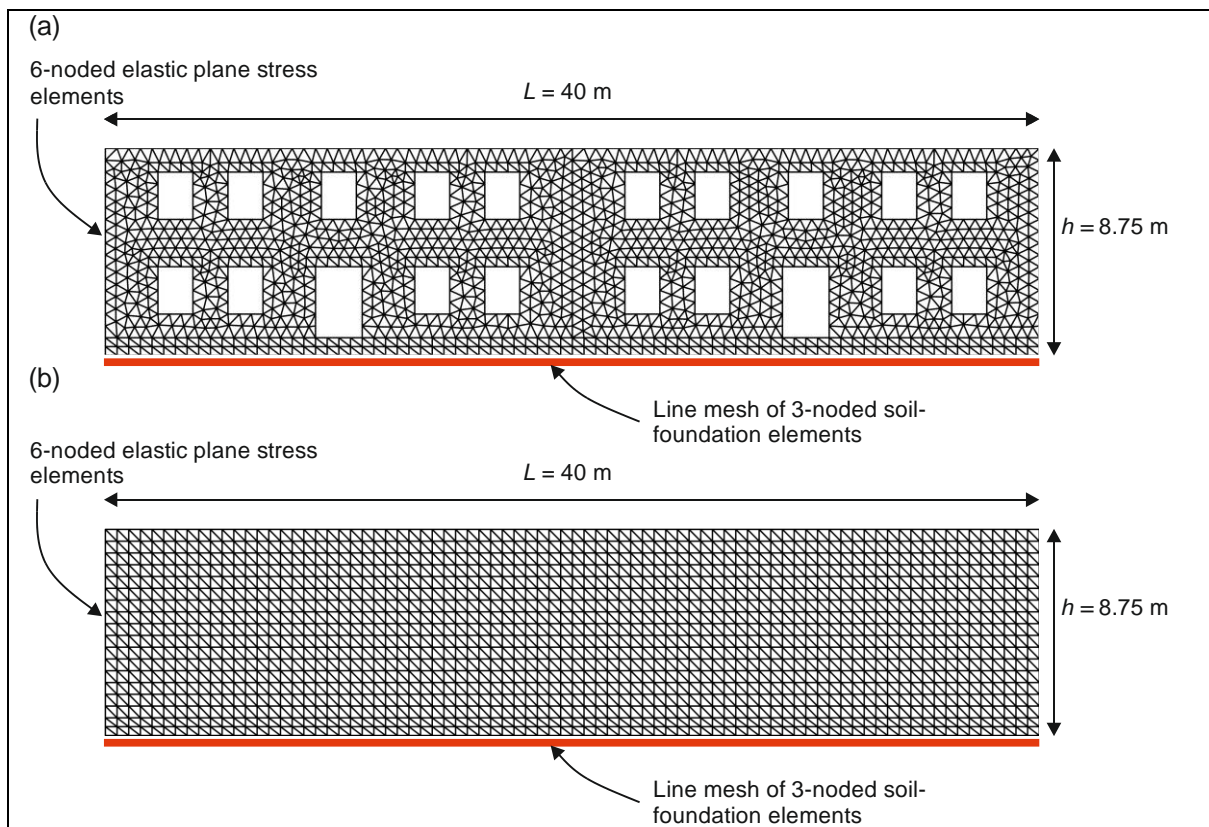
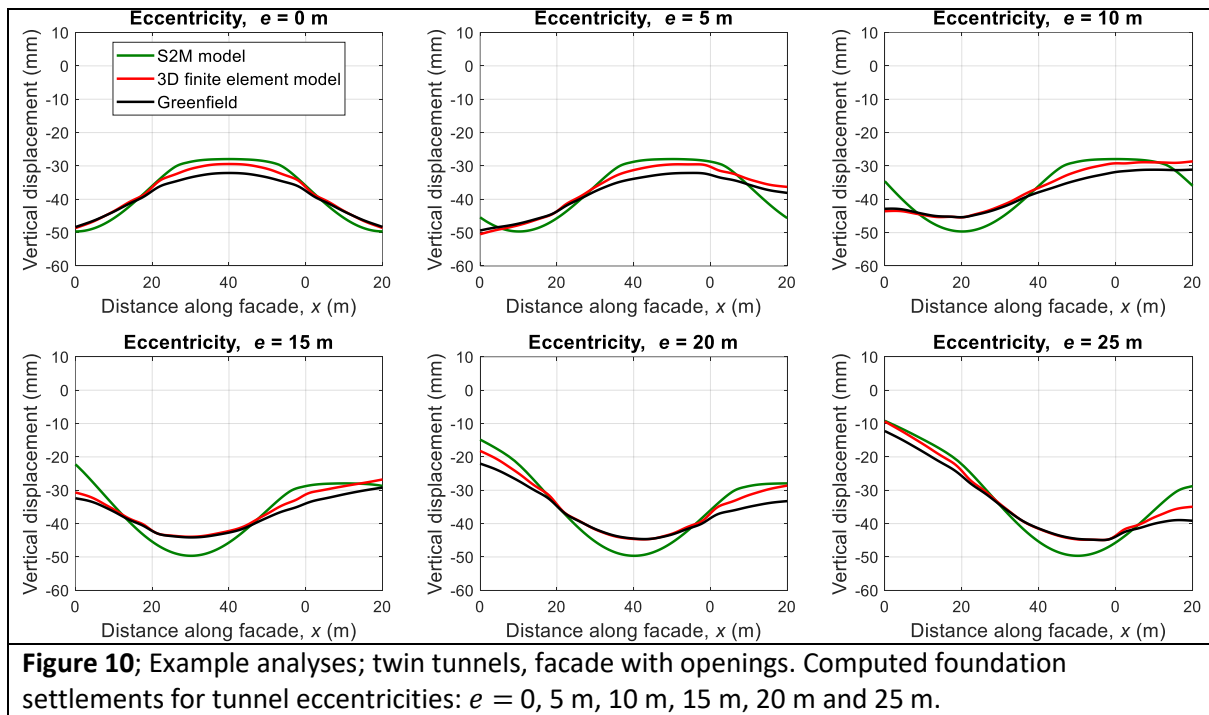
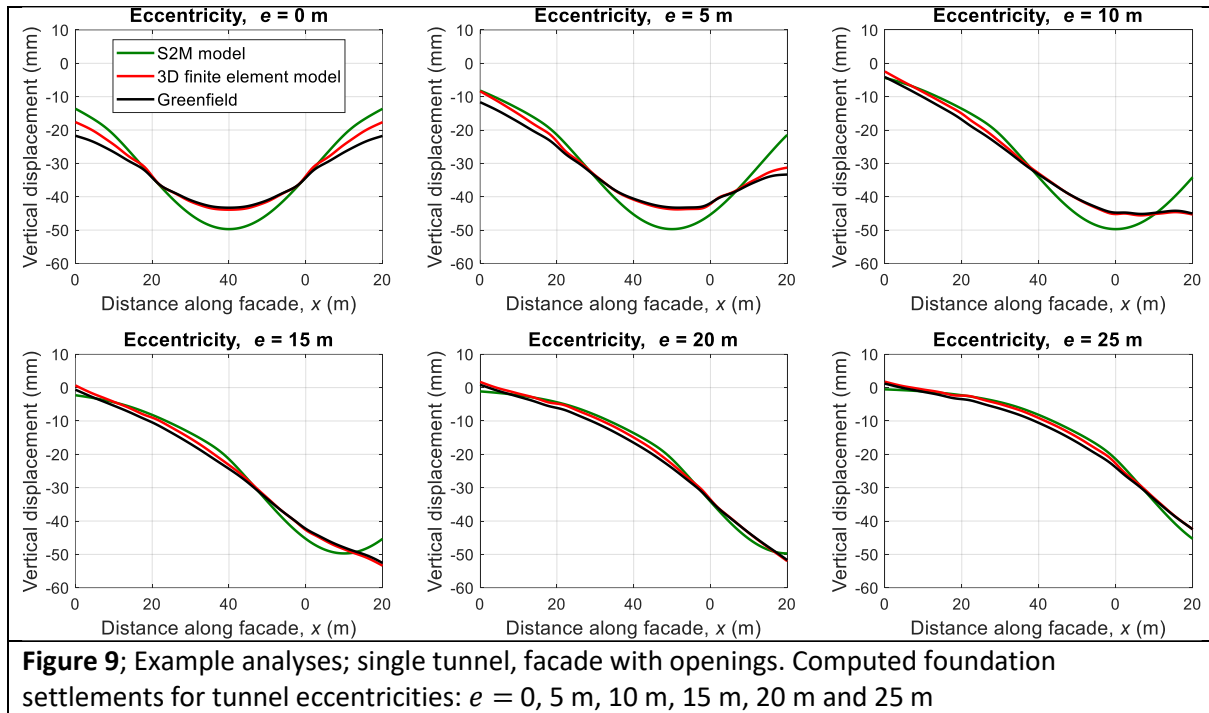


Figure 8; Meshes employed in the S2M for the example analyses: (a) Facade with openings. b) Plain facade. The line mesh of soil-foundation elements (incorporating the combined structural action of the footing and the soil-foundation interaction model) is connected to the nodes at the base of the mesh used to represent the facade.

834



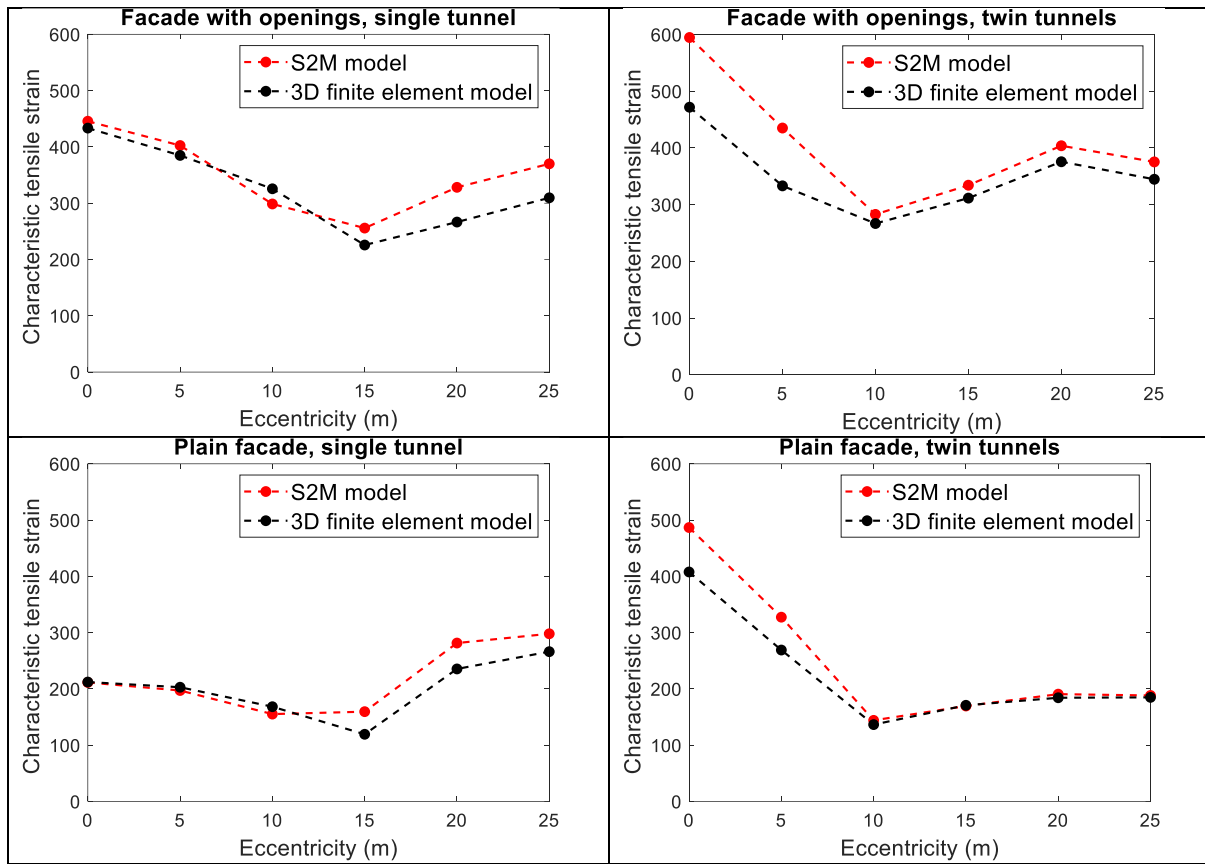
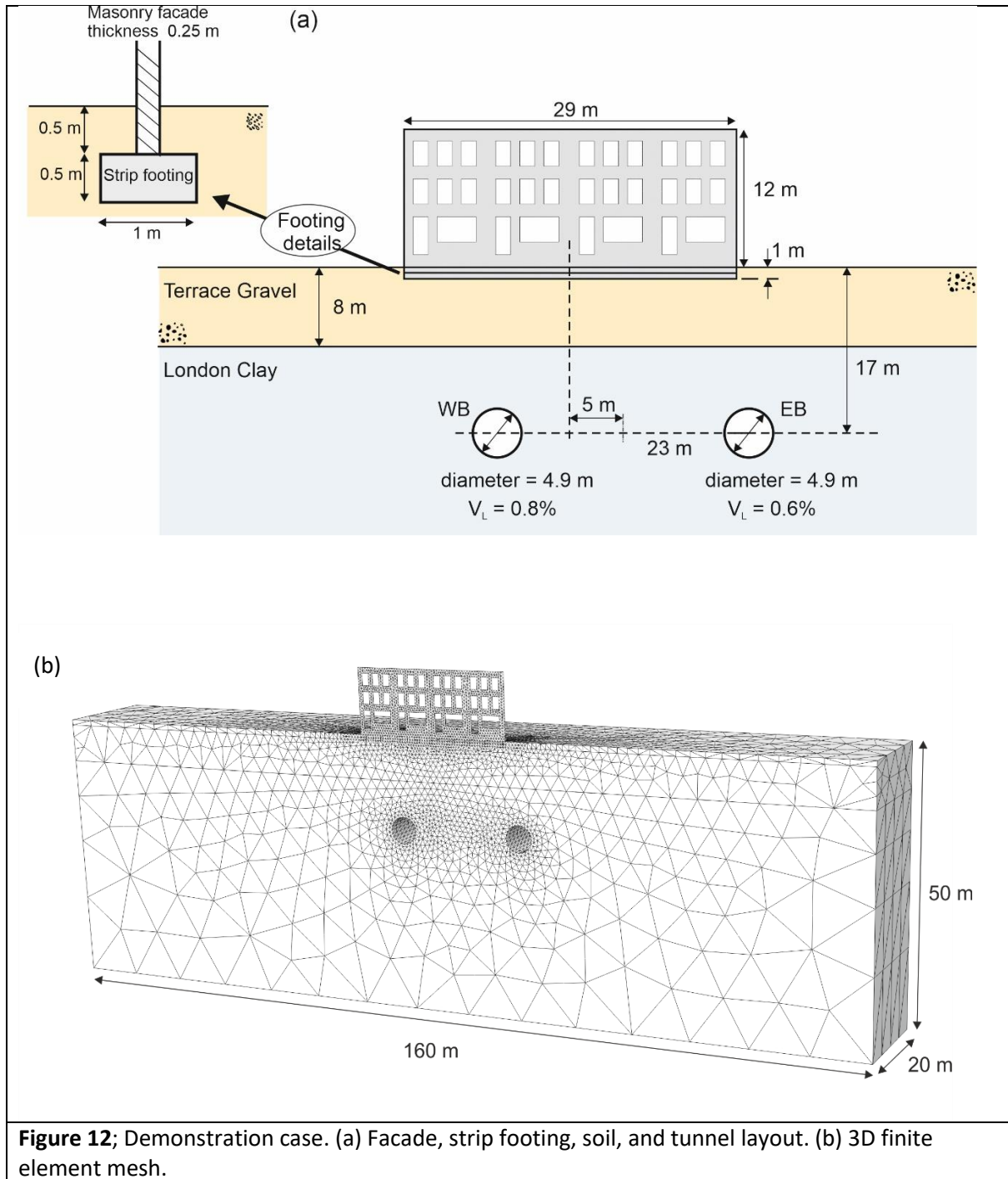
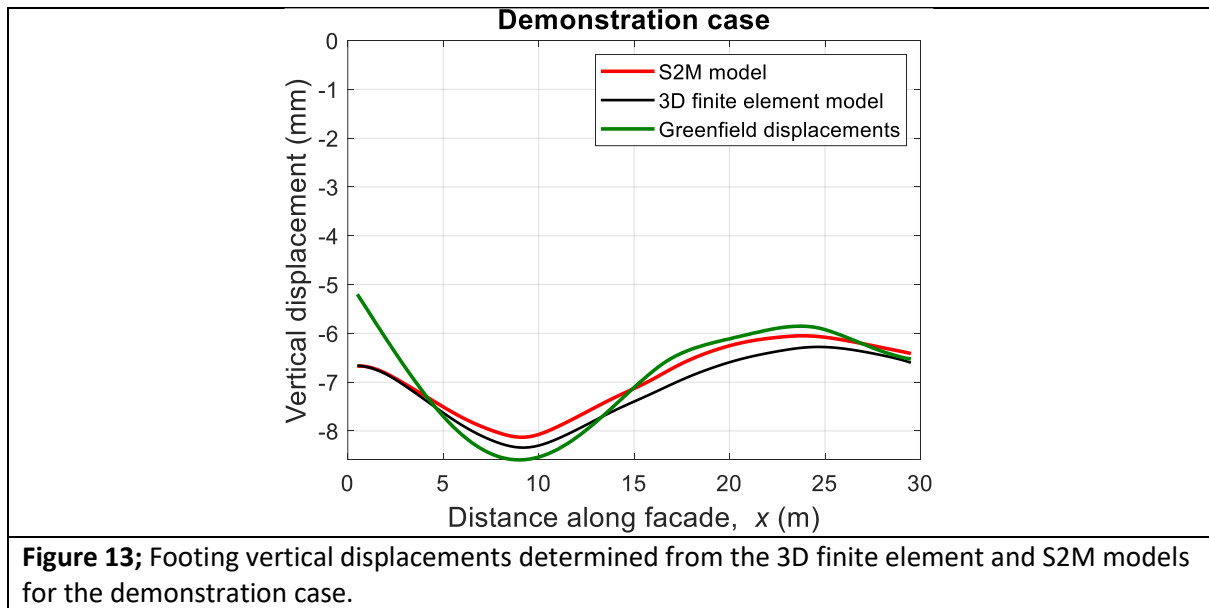


Figure 11; Example analyses; variation of characteristic strain, ε_{99}^t , with tunnel eccentricity. Top – facade with openings; bottom – plain facade. Characteristic strain data have units of microstrain.





849

850

851

852

853